Atomic configuration, conductance, and tensile force of platinum wires of single-atom width

Tokushi Kizuka* and Kosuke Monna
Institute of Materials Science, University of Tsukuba, Tsukuba, Ibaraki 305-8573, Japan
(Received 10 July 2009; revised manuscript received 18 September 2009; published 6 November 2009)

Platinum (Pt) wires of single-atom width were produced by the retraction of a Pt nanotip from contact with a Pt plate at room temperature inside a transmission electron microscope. The distance between the nanotip and the plate was controlled using a conductance feedback system, as a result of which wires showing certain conductance values were observed continuously by *in situ* lattice imaging. Simultaneously, the force acting on the wires was measured using a function of atomic force microscopy. The tip-plate distance was also increased with a constant speed, and the atomic configuration, force, and conductance were similarly investigated. The single-atom-width Pt wires were found to exhibit straight shapes with an interatomic distance of 0.28 ± 0.03 nm. The wires were stable at a tensile force of approximately 1 nN; the observed interatomic distance resulted from elastic expansion. The present study demonstrated experimental evidence for the relationship between wire length and conductance; the wires extend from a three-atom length to a five-atom length as the selected feedback conductance decreases from 2.0 to $0.5G_0$ (where $G_0=2e^2/h$, e being the charge of an electron and h Planck's constant). Contacts exhibiting a conductance of $3.0G_0$ were two-atom-width contacts. In a conductance histogram constructed from the simple retraction, only one peak was observed at $1.3G_0$. Thus, it was found that the conductance of single-atom-width Pt wires is less than $3.0G_0$, with $1.3G_0$ being that of the most-stable state.

DOI: 10.1103/PhysRevB.80.205406 PACS number(s): 61.46.Km, 68.65.La, 68.37.Og, 62.23.Hj

I. INTRODUCTION

Atomic-sized wires (ASWs) are formed at the final stage in the thinning process of nanocontacts (NCs).[1–15] This artificial one-dimensional arrangement of single atoms is unstable; gold (Au) ASWs survive for up to 2 ms at a retraction speed of ~10 nm/s. On the basis of similarity in surface reconstruction, it is proposed that ASWs of the single metallic elements, platinum (Pt) and iridium (Ir), also possess structural stability comparable to that of Au ASWs. The formation process of ASWs during thinning of NCs has been investigated in relation to their quantized conductance defined by a quantum ($G_0=2e^2/h$, where e is the electron charge and h is Planck's constant).[16–26] The histograms of conductance values measured during the thinning process of NCs are produced to examine both the quantization of conductance and corresponding structures. In the conductance histograms of Au NCs, peaks are observed at integer multiples of G_0. The conductance of Au ASWs is related to a unit of G_0, although the conductance deviates owing to irregularities in the wire shape, the convergent angle of electrodes, and the expansion of the interatomic distance.[19,26–28] The geometry and roughness of the contact surfaces including electrodes also contribute to the conductance.[15] In conductance histograms of Pt and Ir NCs, peaks are not observed at quantized values, and the peaks are wider than those of Au NCs.[4,6,7,13,29–37] The deviation from quantized values is interpreted on the basis of inelastic scattering of electrons at 5*d* orbitals.[13,33,38,39] A relationship between the conductance and length of ASWs was reported; for Au, Pt, and Ir ASWs, their conductance oscillates depending on parity in the number of constituent atoms.[13,33,38,39] Furthermore, whereas the average conductance level of Au ASWs is maintained as wire length increases up to the ten-atom length, the average conductance of Pt ASWs decreases with wire length. The atomic configuration of ASWs is examined in association with such conductance features. High-resolution transmission electron microscopy (HRTEM) enables us to observe the atomic configuration directly.[40–50] However, the electrical and mechanical properties of Pt ASWs have not been related directly to the atomic configuration observed by HRTEM.

In this study, we observed the atomic configuration of Pt ASWs by *in situ* HRTEM combined with conductance and force measurements. In particular, Pt ASWs were controlled to maintain a certain conductance using a feedback system to observe corresponding stable structures. From the results of continuous observation of the structures on an atomic scale, we demonstrate experimental evidence for the relationships between the atomic configuration, conductance, and mechanical properties of Pt ASWs.

II. EXPERIMENTAL METHODS

The experimental method in this study was developed on the basis of *in situ* HRTEM combined with subnanonewton force measurements used in atomic force microscopy (AFM) and electronic-conductance measurements used in scanning tunneling microscopy.[46,50] First, we prepared Pt nanotips: Pt was evaporated in a vacuum chamber and deposited on a Si cantilever with a nanotip for AFM. The cantilever tip was attached to the front of a tube piezoelement on a cantilever holder for HRTEM. A Pt plate 0.2 mm in thickness was attached to a plate holder. The contact edge of the plate was thinned to 5–20 nm by argon ion milling. The cantilever and plate holders were then inserted into the transmission electron microscope at the University of Tsukuba. The specimen chamber of the microscope was evacuated first by a turbomolecular pump and then by an ion pump, resulting in a vacuum of 1×10^{-5} Pa with typical residual gaseous mol-

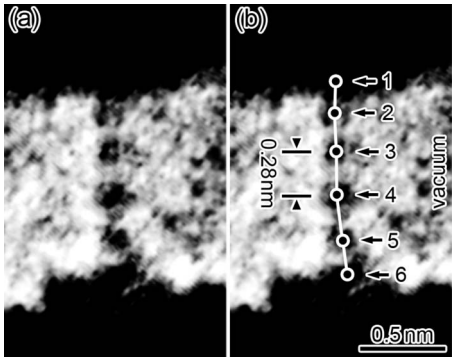

FIG. 1. (a) High-resolution image of a Pt wire of single-atom width during retraction while a direct-current voltage of 13 mV was applied. The position of atoms is shown in (b). The cantilever tip and the plate are seen in the upper and lower regions of the frame, respectively. The ASW is located between the tip and the plate. The brighter area around the wire is the vacuum. The image contrast was increased to show the wire clearly, as a result of which the tip and plate regions appear with lower intensities.

ecules of H_2, O_2, H_2O, CO, CO_2, N_2, and hydrocarbon. The cantilever tip was brought into contact with the edge surface of the opposing plate by piezomanipulation while applying a bias voltage of 13–30 mV between the cantilever tip and the plate. The cantilever tip was next pressed into the plate edge to prepare NCs and then retracted to elongate them. In addition to this simple contact-retraction manipulation, we controlled the operating voltage of the piezoelement connected to the cantilever, i.e., the distance between the cantilever tip and the plate, using a conductance feedback circuit, as a result of which Pt NCs and ASWs showing a certain conductance were observed continuously. A series of these manipulations were performed at room temperature. The structural dynamics during the process was observed *in situ* by HR-TEM lattice imaging using a television capture system. The time resolution of image observations was 17 ms. The force acting on the contacts was simultaneously measured by optical detection of cantilever deflection. The electrical conductance was measured using a two-terminal method. The results of high-resolution imaging and signal detection in this system were simultaneously recorded and analyzed for every image.

III. RESULTS

Figure 1(a) shows a high-resolution image of a Pt ASW produced by simple retraction of a Pt NC. The cantilever tip was separated from the plate with a speed of 0.7 nm/s. The conductance feedback circuit was not used for the observation of the image shown in Fig. 1. The ASW is composed of six atoms with an interatomic distance of 0.28 ± 0.03 nm, as shown in Fig. 1(b). The force acting on the ASW was 0.8 ± 0.2 nN. Thus, the observed interatomic distance is that under this force. The conductance of this ASW was $0.2G_0$.

Figures 2(a)–2(d) show high-resolution images of Pt wires during conductance feedback control. The bias voltage applied to the wires was 13 mV. The feedback conductance was selected to be 0.5, 1.0, 2.2, and $3.0G_0$ for Figs. 2(a)–2(d), respectively. The wires are observed as dark vertical lines connecting the cantilever tip in the upper region and the plate in the lower region of each frame. The width of the wires shown in Figs. 2(a)–2(c) corresponds to single-atom wide; these are ASWs. The wire length is 0.54 ± 0.10, 0.80 ± 0.05, and 1.15 ± 0.05 nm for the ASWs in Figs. 2(a)–2(c), respectively. On the other hand, the width of the wire shown in Fig. 2(d) corresponds to two atoms at a feedback conductance of $3.0G_0$. Individual atoms in the wires are not identified in Figs. 2(a)–2(d), whereas atoms are clearly observed in the ASW shown in Fig. 1. This is because during feedback control, the cantilever tip vibrated along the wire direction to adjust the conductance.

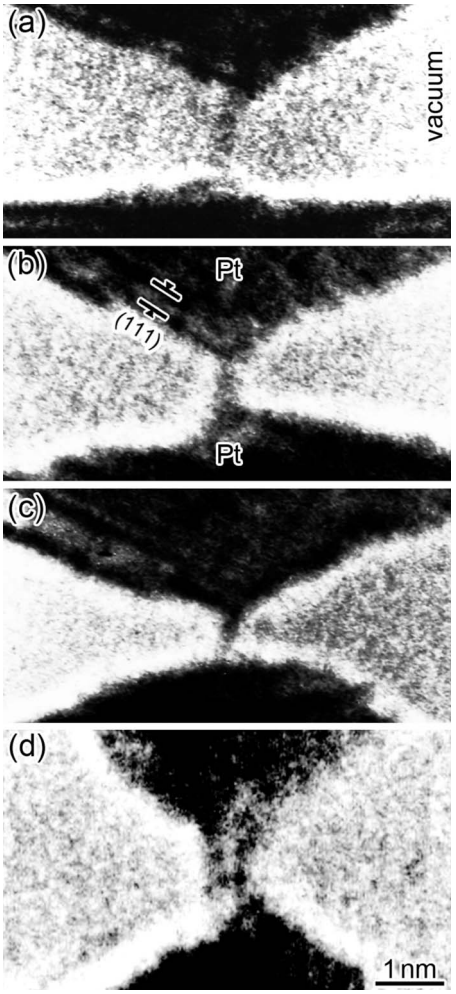

FIG. 2. High-resolution images of Pt wires of single-atom width [(a)–(c)] and two-atom-width [(d)] during conductance feedback control. The bias voltage applied to the wires was 13 mV. The feedback conductance was selected to be 0.5, 1.0, 2.2, and $3.0G_0$ for (a), (b), (c), and (d), respectively. The wires are observed between the tip in the upper region of each frame and the plate in the lower region. The (111) lattice fringes appearing in the tip are indicated in (b). The brighter area is the vacuum. The contrast was increased to show the wires clearly; as a result, the tip and plate regions appear with lower intensities.

Figure 3 shows the variation in the conductance of, and force acting on, the Pt ASWs and two-atom-width wire during conductance feedback control. The recorded signals dis-

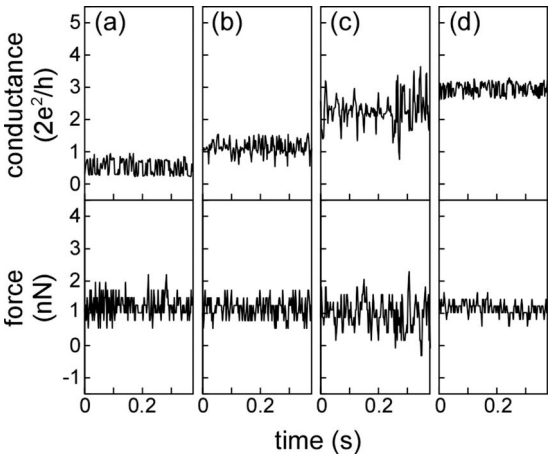

FIG. 3. Conductance of, and force acting on, the Pt wires of single-atom width [(a)–(c)] and two-atom-width [(d)] presented in Figs. 2(a)–2(d) during conductance feedback control. The feedback conductance was selected to be 0.5, 1.0, 2.2, and $3.0G_0$ for (a), (b), (c), and (d), respectively.

tribute around the selected conductance values, showing that the feedback system behaved properly. For the ASWs, the fluctuation in the conductance becomes larger as the assigned value increases, as shown in Figs. 3(a)–3(c). For the wire of two-atom width, the deviation from the assigned value ($3.0G_0$) is the minimum. The fluctuation of the force increases when the conductance value deviated from the assigned value. In particular, in an assigned conductance of $2.2G_0$, the force peaks and dips exceed twice the assigned value. At such a large force variation, the structure of the contact fluctuated owing to the control of the tip-plate distance by the feedback system. Typical ASWs, as presented in Fig. 2, were observed when the conductance value was converged around the assigned value.

Figures 4(a)–4(d) show the conductance histograms produced from measurements during the conductance feedback control of the Pt wires presented in Figs. 2(a)–2(d). The feedback conductance values were 0.5, 1.0, 2.2, and $3.0G_0$ for Figs. 4(a)–4(d), respectively. As also seen in Fig. 3, the counts distribute around the selected conductance. In particular, in the histograms for feedback conductances of 1.0, 2.2, and $3.0G_0$ in Figs. 4(b)–4(d), each main peak corresponds to the feedback value. On the other hand, certain levels of counts are observable outside of the feedback values, i.e., at $0.2G_0$ in Fig. 4(b) and around $1.3G_0$ in Fig. 4(c). In addition, the peak at $1.0G_0$ in Fig. 4(b) exhibits an asymmetric distribution, involving a small amount of additional component around $1.3G_0$. In the histogram for a feedback conductance of $0.5G_0$ in Fig. 4(a), two peaks are observed at 0.3 and $0.7G_0$, deviating from the feedback value. Figure 4(e) shows a histogram of conductance values measured during thinning of Pt NCs to ASWs without using the feedback system. A peak is seen at $1.3G_0$ with a gently undulating distribution at other conductance levels. The $1.3G_0$ peak corresponds to the main peak observed in conductance measurements of Pt contacts by Smit *et al.*[32,51] (1.4–1.8 and $1.3–1.5G_0$) and by Untiedt *et al.*[36] ($1.5G_0$), and is similar to that reported by Yuki *et al.*[29] ($1.7G_0$) and Shiota *et al.* ($1.7G_0$).[37]

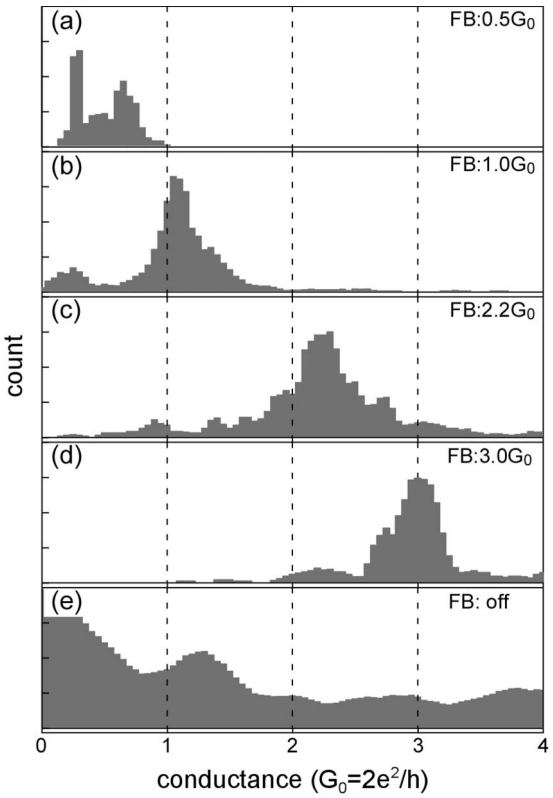

FIG. 4. Histograms of conductance values measured during conductance feedback control of the Pt wires [(a)–(d)] presented in Figs. 2(a)–2(d) and a simple thinning-breaking process of Pt nanocontacts without using feedback control [(e)]. The feedback conductance values were (a) 0.5, (b) 1.0, (c) 2.2, (d) and $3.0G_0$, as indicated by the vertical dashed lines. Peaks are seen at 0.3 and $0.7G_0$ in (a), at 0.2 and $1.0G_0$ in (b), at $2.2G_0$ in (c), at $3.0G_0$ in (d), and at $1.3G_0$ in (e).

Figure 5 shows histograms of the force acting on the Pt wires during conductance feedback control. The measured force values distribute from 0 to 1.5 nN for the ASWs, as shown in Figs. 5(a)–5(c). For the two-atom-width wire, the distribution width is similar, as shown in Fig. 5(d). Although the force distributions for all wires in Fig. 5 overlapped, the peak position for a feedback conductance of $2.2G_0$ is 0.3 nN smaller than those of 0.5 and $1.0G_0$. The wire length decreased with the feedback conductance value. Thus, larger tension is applied to longer ASWs. For the two-atom-width wire, the force distribution is similar to that of the longer ASWs, as shown in Fig. 5(d).

Figure 6 shows the relationship between the conductance and wire length of the Pt ASWs during feedback control. The distribution of the wire length is shown in the upper frame. Four peaks are observed in this distribution. The differences in length between the peak positions are 0.27, 0.25, and 0.31 nm. The average of these values is 0.28 nm, which is comparable to that of the ASW presented in Fig. 1. We defined this length as the interatomic distance because the atomic position of ASWs in Fig. 2 was not identified owing to continuous adjustment of the tip-plate distance. Using the average interatomic distance, we determined the lower lateral axis of Fig. 6, i.e., the wire length of the ASWs, and the

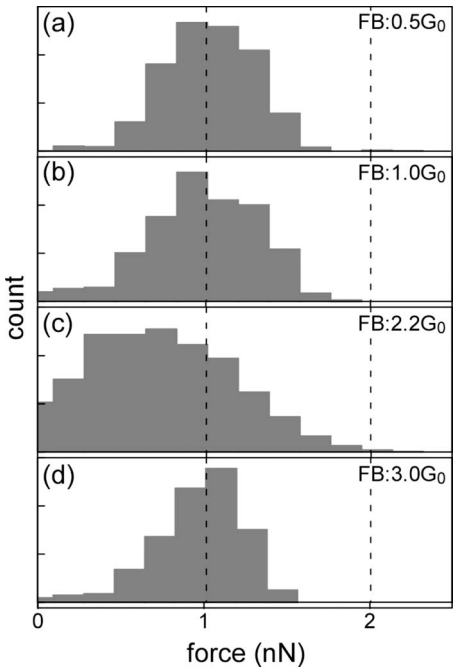

FIG. 5. [(a)–(d)] Histograms of force acting on the Pt wires presented in Figs. 2(a)–2(d), respectively, measured during conductance feedback control. The controlled conductance was (a) 0.5, (b) 1.0, (c) 2.2, and (d) $3.0G_0$. Peaks are seen at 1.1 ± 0.4 nN in (a), 1.0 ± 0.4 nN in (b), 0.7 ± 0.6 nN in (c), and 1.1 ± 0.3 nN in (d).

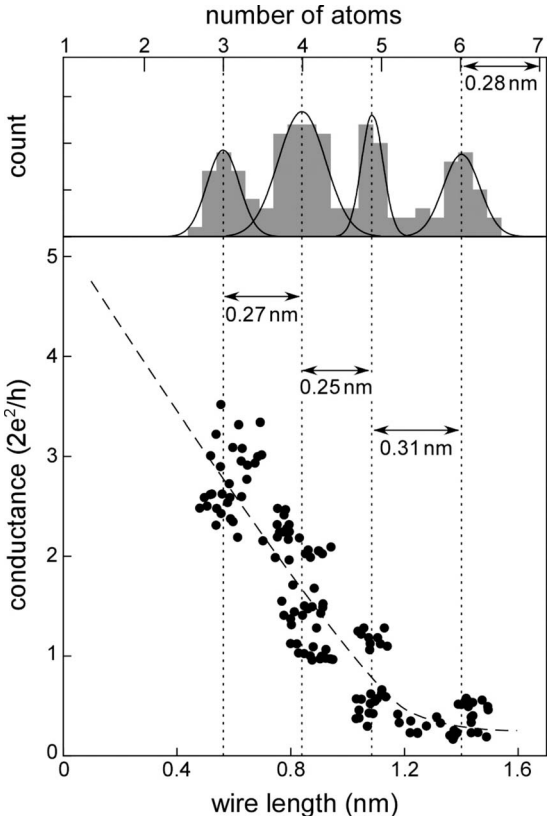

FIG. 6. Relationship between conductance and wire length of the Pt wires presented in Figs. 2(a)–2(d) during conductance feedback control (lower frame) and histogram of wire length values (upper frame). Solid curves represent fitted Gaussian functions for each peak in the wire-length distribution. The separation of the peaks in the histogram is 0.27, 0.25, and 0.31 nm, with an average of 0.28 nm. The number of atoms estimated using an interatomic distance of 0.28 nm is indicated on the upper lateral axis. Dashed line in the lower frame represents an approximate line by eyes.

number of atoms shown on the upper lateral axis. The conductance is found to decrease as the wire length increases. Similar relationships were observed by Smit *et al.*[51] using a scanning tunneling microscope and a mechanically controllable break junction technique. From first-principles simulation and density-functional theory, García-Suárez *et al.*[39] also obtained a similar relationship. These experimental and theoretical studies result in the parity oscillation of conductance during extension of Pt ASWs. However, in Fig. 6, the parity oscillation is indistinct, probably owing to tip vibration.

Figure 7(A) shows a time-sequence series of high-resolution images of thinning from Pt NC to ASW by simple retraction with a speed of ~0.5 nm/s without using the conductance feedback system. During this process, we applied an alternate-current voltage of 30 mV with a frequency of 20 Hz between the tip and the plate. The NC and ASW are observed between the tip in the upper region and the plate in the lower region of each frame in Fig. 7(A). A simulation of high-resolution imaging of ASWs confirmed that the atoms of the ASW appear as black dots in the intensity image at the Scherzer focus condition.[50,52] Furthermore, the centers of the atoms correspond to those of the black dots within a deviation of 0–0.02 nm.[50] We constructed models of the atomic configurations viewed along the observation direction, as shown in Fig. 7(B). The image simulation also shows that the darkness at the atom positions of ASWs corresponds to the thickness, i.e., the number of atoms aligning along the observation direction. We measured the line intensity of the high-resolution images in Fig. 7(A) along the minimum width of the constriction region, as shown in Fig. 7(C). The darkness was found to correspond to three levels, i.e., the vacuum level and two equally spaced levels, as indicated by broken lines in Fig. 7(C). From this line intensity, we constructed models of the atomic configuration on the cross-section at the minimum width of the constricted regions, as shown in Fig. 7(D). In accordance with these models, we identified three ASWs, as shown in Figs. 7(f)–7(h). The wire is composed of three atoms for the ASWs in Figs. 7(f) and 7(g) and of four atoms for that in Fig. 7(h). The geometry and roughness of the contact surfaces including electrodes also contribute to the conductance.[15] In our observation, both the wire part and electrodes are observed at an atomic resolution.

The thinning of the contact in Fig. 7 is explained based on the models. As shown in Figs. 7(a)–7(e), the NC became thinner as it was retracted; the number of atoms on the minimum cross-section decreased from six to two. Owing to subsequent retraction, the number of atoms further decreased to one, i.e., an ASW with a three-atom length formed [Fig. 7(f)]. The direction of the ASW was tilted from the retraction direction. High-resolution imaging showed that after the elongation and tilting of the ASW, the tip approached the plate spontaneously even though tensile force acted. As a result, the wire tilted toward the retraction direction: the wire

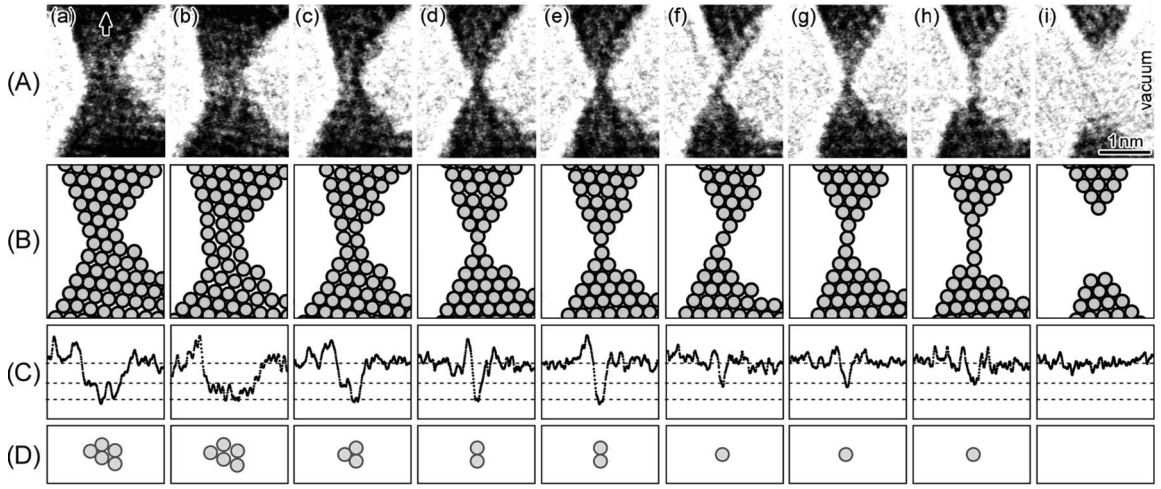

FIG. 7. (A) Time-sequence series of high-resolution images of thinning from a Pt nanocontact to a single-atom-width wire by retraction while applying an alternate-current voltage of 30 mV with a frequency of 20 Hz. The cantilever tip was separated from the plate with a speed of ~0.5 nm/s. (The tip-plate distance was not controlled by the conductance feedback circuit.) The nanocontact and wire are located between the tip in the upper region of each frame and the plate in the lower region. The image contrast was increased to show the contact and wire clearly; as a result, the tip and plate regions appeared with lower intensities. The brighter area corresponds to the vacuum. (B) The configuration of atoms along the observation direction, corresponding to the high-resolution images in (A). (C) The line intensity of the high-resolution images in (A) along the minimum width of the constriction region. Broken lines represent three darkness levels, i.e., the vacuum level and two equally spaced levels. (D) Models of the atomic configuration of the cross-section at the minimum width.

direction recovered [Fig. 7(g)]. Subsequently, the ASW elongated to a four-atom length owing to the tensile force [Fig. 7(h)]. Finally, the ASW broke [Fig. 7(i)].

Figure 8 shows the variation in the tip-plate distance, the minimum contact width at nanometer scale (left) and the number of atoms (right), force and stress acting on the contact, conductance of the contact, and conductance per atom, as functions of time. To calculate stress, we assumed that the minimum cross-sectional area of the contact was circular. In particular, the cross-sectional area of a single atom in a rigid sphere model for bulk Pt is used as that of the ASW ($0.060\ \mathrm{nm}^2$). Times indicated by arrows a–h in Fig. 8 correspond to those of Figs. 7(a)–7(h). The tip-plate distance increases in a stepwise fashion, as shown in the top frame of Fig. 8. With this stepwise variation, the minimum cross-sectional width decreases. Both the force acting on the contact and the conductance decrease rapidly at the time of each stepwise increase in the tip-plate distance. These show that mechanical yield behavior occurred in the contact during retraction: three slips in the NC from Fig. 7(a) to Fig. 7(f) and the extraction of an atom in the ASW from Fig. 7(g) to Fig. 7(h).

The stress observed in Fig. 8 ranges from 3 to 9 GPa. The fracture of the ASW occurred around the maximum stress. The stress is comparable with that observed for Au ASWs (8–17 GPa).[50]

In the time-force curve in Fig. 8, gradually increasing periods are observed before the force rapidly decreases, corresponding to elastic elongation. Owing to this elastic elongation, the conductance slightly decreases during the periods, as shown in time a–e in Fig. 8. Such a force-conductance relationship is well known for Au ASWs. However, note that the opposite relationship is observed in time f and g. This period corresponds to the tilting of the ASW, as shown in Figs. 7(f) and 7(g).

The stress-strain relationship for the elastic-elongation procedure of the longest ASW [Fig. 7(h)] was obtained from Fig. 8, as shown in Fig. 9. From the average gradient of the curve, the Young's modulus of the ASW was calculated to be 33 ± 5 GPa. It was reported that the Young's modulus of Au ASWs is 47–116 GPa.[50] From the elongation length and corresponding farce increase in time f and g, we estimated the stiffness of the three-atom Pt ASW observed to be 5 ± 1 N/m. This value is at least six times larger than the stiffness of Pt ASWs with the same length (0.8 N/m),[37] whereas it is comparable with a stiffness of Au ASWs (5.8 N/m).[5]

As shown in Fig. 8, the conductance per atom at the minimum cross-sectional area ranges from 1.5 to 2.5 for the NCs. After the NC transformed into the ASW, its conductance decreases to less than $0.2G_0$, implying that electron inelastic scattering is changed by this structural transformation.

Figure 10 shows the current-voltage curves of the NC and ASW presented in Figs. 7(a), 7(c), 7(e), 7(g), and 7(h). The curves deviate from linear relationships at higher voltages. As previously done by Nielsen *et al.*,[13] we fitted the current-voltage curves of the contact presented in Figs. 7(a)–7(h) with third-order polynomials, $I_{\mathrm{total}}=G^{(1)}V+G^{(2)}V^2+G^{(3)}V^3$ (I_{total}: the total current; V: bias voltage; $G^{(1)}$, $G^{(2)}$, and $G^{(3)}$: coefficients of the first-, second-, and third-order terms corresponding to the conductance components of lower bias voltages, the polarity dependence of the asymmetry of the contact structure and nonlinearity, respectively). Figure 11 shows these coefficients, the ratio $G^{(3)}/G^{(1)}$, and I of each term, $G^{(1)}V$, $G^{(2)}V^2$, and $G^{(3)}V^3$, against conductance. As shown in the variation in I, the $G^{(1)}V$ component dominates the total current (for $V=30$ mV, the ratio of $G^{(2)}V^2$ and $G^{(3)}V^3$ to the total current is ~0.1%).

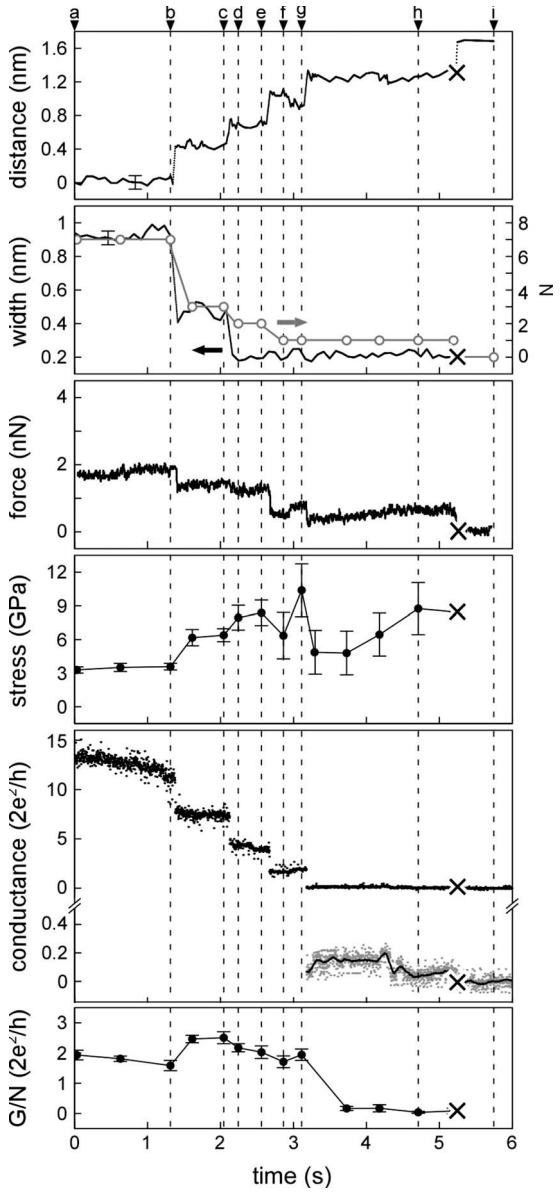

FIG. 8. Variation in the tip-plate distance, the minimum contact width at nanometer scale (left) and the number of atoms (right), force and stress acting on the contact, conductance of the contact, and conductance per atom, as functions of time. Times indicated by arrows a–h correspond to those of Figs. 7(a)–7(h). The crosses ($\times$) show fracture. The conductance from time g to time h is shown with an enlarged scale.

IV. DISCUSSION

A. Elastic elongation of Pt ASWs and interatomic distances

First, we note that all measured forces acting on NCs and ASWs were positive, as shown in Fig. 5; tensile forces were needed to maintain the ASW structures corresponding to selected conductances from 0.5 to $3.0G_0$. This reveals that the ASWs elongated elastically. The force distribution for the ASWs in Figs. 5(a)–5(c), measured in the elastic-deformation region, is smaller than the breaking force acting on straight periodic Pt ASWs calculated by Bahn and Jacobsen (3.9 nN).[53] Thus, the interatomic distances observed in this study (0.28 nm in Fig. 1 and 0.27, 0.25, and 0.31 nm, with an average of 0.28 nm, in Fig. 6) are those elastically elongated by tensile forces. If we suppose the elastic strain to be ~0.1 from the result in Fig. 9, the interatomic distance at stress-free states is calculated to be ~0.25 nm. This value is similar to that measured by the mechanically controllable break junction technique[51] and calculated using molecular dynamics and density-functional theory by Bahn and Jacobsen.[53] However, we point out that the stress-free states are not necessarily the most stable for straight-wire structures. At such states, unstable ASWs may transform to other structures (zigzag structures or clusters).

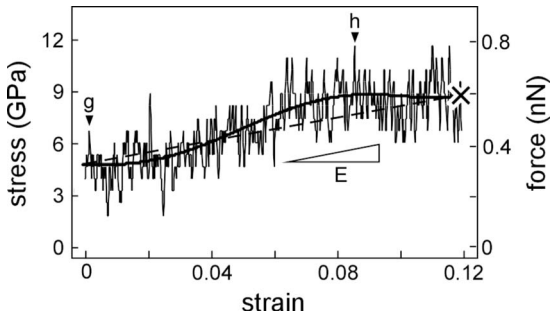

FIG. 9. Stress-strain relationship of the longest atomic-sized wire observed before breaking. Force corresponding to stress is also shown on the right vertical axis. The observed points of high-resolution images shown in Figs. 7(g) and 7(h) are indicated. Solid and broken lines represent polynomial and linear approximated curves, respectively. The gradient of the linear approximation corresponds to the average Young's modulus of the wire (E) (33 ± 5 GPa). The cross indicates fracture.

B. Stability of Pt ASWs and their conductances

As shown in Fig. 2, the contacts exhibited ASW structures when the feedback conductance value was selected to be less than $3G_0$. Thicker contacts, e.g., NCs of two atoms wide,

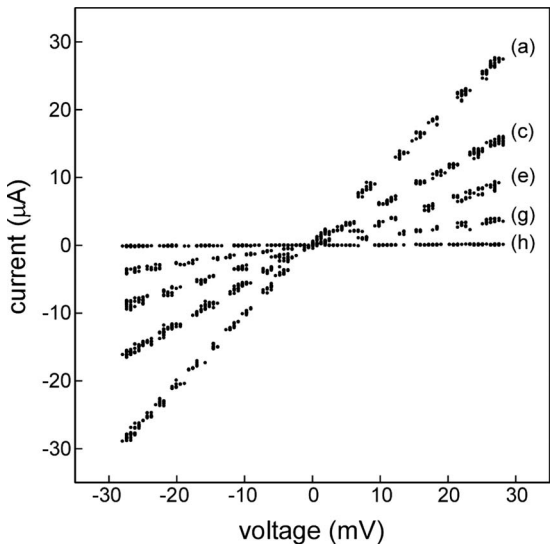

FIG. 10. Current-voltage curves of the nanocontact and single-atom-width wire presented in Figs. 7(a), 7(c), 7(e), 7(g), and 7(h). The conductance at 0 V is 13, 7.5, 3.9, 2.0, and $0.1G_0$ for curves (a), (c), (e), (g), and (h), respectively.

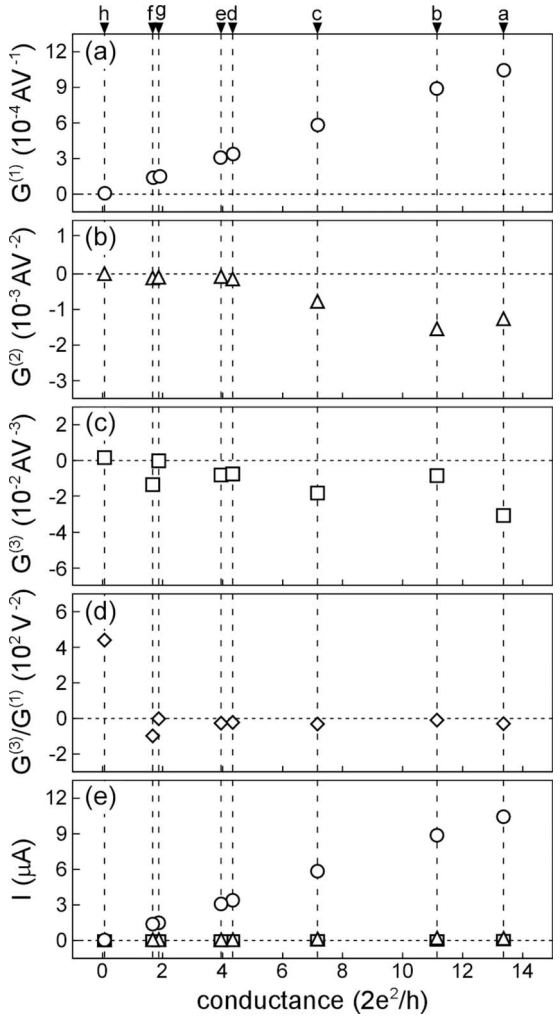

FIG. 11. Coefficients of polynomials ($I_{total}=G^{(1)}V+G^{(2)}V^2+G^{(3)}V^3$; I_{total}: total current; V: bias voltage; $G^{(1)}$, $G^{(2)}$, and $G^{(3)}$ are coefficients of the first-, second-, and third-order terms) fitting the current-voltage curves of the contact presented in Figs. 7(a)–7(h), the ratio $G^{(3)}/G^{(1)}$, and I of $G^{(1)}V$, $G^{(2)}V^2$, and $G^{(3)}V^3$ against conductance.

appeared for a higher feedback conductance, $3G_0$. Thus, the conductance of Pt ASWs is found to be less than $3G_0$. Details of the stability of ASWs possessing certain conductance values can be discussed on the basis of the conductance histograms during feedback control. In the histogram for a feedback conductance of $0.5G_0$ in Fig. 4(a), two peaks were observed at 0.3 and $0.7G_0$, both deviating from the feedback value. Furthermore, at $0.3G_0$ in the histogram for a feedback conductance of $1.0G_0$ in Fig. 4(b), a certain level of counts was observable outside of the feedback value, whereas the main peak corresponds to the feedback value. Thus, we note that ASWs exhibiting 0.3 and $0.7G_0$ formed preferentially even though the feedback system controlled the conductance to other values; the 0.3 and $0.7G_0$ ASWs are more stable than the ASWs of the selected conductances. In addition, for a feedback conductance of $1.0G_0$, a small amount of component around $1.3G_0$ contributing to an asymmetric distribution was observed around the main peak at $1.0G_0$, as shown in Fig. 4(b). A peak at $1.3G_0$ was also observed in the conductance histogram for the simple thinning process shown in Fig. 4(e); the $1.3G_0$ ASWs are the most stable without feedback control. Therefore, the ASWs possessing these conductances, i.e., 0.3, 0.7, and $1.3G_0$, are more stable than ASWs corresponding to the other conductance levels.

C. Structure and conductance of pure and hydrogen-incorporated Pt ASWs

It is well known that Pt ASWs incorporate hydrogen molecules.[29,32,54,55] As previously reported, peaks are observed at $1.3-1.8G_0$ in conductance histograms when pure Pt NCs are retracted in ultrahigh vacuum.[32,36,37] On the other hand, peaks near 0.2 and $\sim 0.9G_0$ are observed beside a trough near $0.5G_0$ when Pt NCs are examined in a hydrogen atmosphere.[32,55] In accordance with these previous results, we classified the Pt ASWs observed in this study, since a hydrogen molecules is not imaged by HRTEM (Ref. 52); pure Pt ASWs exhibiting conductances exceeding $1.3G_0$ and hydrogen-incorporated Pt ASWs exhibiting conductances less than $\sim 0.9G_0$. In Fig. 4(a), although a feedback conductance of $0.5G_0$ was selected, the intensities of both the 0.3 and $0.7G_0$ levels were higher. It is also noted that in the relationship between the wire length and conductance in Fig. 6, the differential of the approximated curve rapidly changes around 1 nm in wire length, which corresponds to the ASWs possessing 0.3 and $0.7G_0$. Hydrogen molecules were the major residual gaseous molecules in the specimen chamber. These results suggest that the 0.3 and $0.7G_0$ ASWs were stabilized by the incorporation of hydrogen molecules. Similarly, it is inferred that the ASW exhibiting $0.2G_0$ observed during simple retraction (Fig. 1) and the ASW exhibiting $1G_0$ observed during the feedback control [Fig. 2(b)] are hydrogen-incorporated Pt ASWs. A pure Pt ASW is deduced to be the shortest ASW in the feedback control with an assigned value of $2.2G_0$ [Fig. 2(c)]. The ASW observed during simple retraction, presented in Fig. 7, showed first $1.7G_0$ (time f and g) and then showed a conductance less than $0.2G_0$ (time g and h). Therefore, we infer that first a pure Pt ASW was formed and then it incorporated hydrogen molecules.

D. Relationship between the conductance and length of Pt ASWs

In both feedback control and simple retraction, the conductance of the ASWs decreases as their length increases, as shown in Figs. 6 and 8. Such a relationship was found previously in experimental and theoretical studies of Pt ASWs. The slope of the approximated curve in Fig. 6, i.e., the decrement rate of conductance against the wire length, is $-4G_0/\mathrm{nm}$. This decrement rate is two to four times larger than that previously observed by using piezo displacement.[51] In this study, the wire length in Fig. 6 was directly determined from HRTEM. Thus, the difference in the decrement rate may be due to the definition of the wire length.

The relationship between conductance and wire length is unexpected for a ballistic wire in which conductance is constant against its length, as typically discussed in Au ASWs having the $6s$ channel. For Pt ASWs, the partially filled $5d$

multichannels dominate their conductance.[13,33,38,39] As the spatial distribution of the 5*d* electrons is localized, wire expansion causes a larger change in the distribution. de la Vega *et al.*[38] showed from a first-principles calculation that the conductance of a Pt ASW composed of eight atoms decreases by $0.5G_0$ when the interatomic distance increases by 0.01 nm from 0.28 nm, corresponding to a strain increase of ~0.04. According to an *ab initio* calculation by Nielsen *et al.*,[33] the conductance of a Pt single-atom contact decreases from 2.1 to $1.1G_0$ as the interatomic distance increases from 0.27 to 0.35 nm. As shown in Fig. 8, during simple retraction of Pt ASWs, the strain increases up to ~0.1 with increasing wire length. For feedback control, larger retraction distances are needed to form longer ASWs. Thus, an increase in the ASWs' strain is related to the reduction in conductance. For the ASWs exhibiting a conductance larger than $1G_0$, corresponding to a linear relationship between conductance and length, the decrease in the overlap of electronic states due to straining may contribute to the reduction in conductance, as discussed by Smit *et al.*[51] For longer ASWs exhibiting a conductance of less than $1G_0$, the influence of hydrogen incorporation should be considered for the conductance reduction, as discussed in Sec. IV C.

E. Channel number of Pt single-atom contacts

In the feedback control, the ASWs' length is reduced to a length of approximately three atoms for a feedback conductance of $2.2G_0$. Shorter ASWs, i.e., single-atom contacts and dimer ASWs, were not observed in this study, since the contact structure transformed to NCs of two-atom width when the feedback conductance exceeded $3G_0$. However, in simple retraction of contacts without feedback control, various thinning processes are realized, and such single-atom contacts and dimer ASWs are formed inevitably at the transformation from NCs to ASWs. We deduce the conductance of these shorter ASWs from the relationship between the conductance and wire length in Fig. 6. When the relationship is fitted with a linear function for wire lengths shorter than 0.9 nm, the extrapolation to zero wire length, which corresponds to single-atom contacts, crosses at a conductance of $\sim 5G_0$. At this zero wire length, electron inelastic scattering through the contact decreases to the minimum; the transmission probability in each channel increases. As shown by García *et al.*,[15] in addition to the geometry of ASWs, the shape and roughness of the electrodes contribute to electron inelastic scattering. For the present ASWs, it has not been shown whether all *d* channels perfectly open in the limit of zero wire length. The channel number of the zero-length Pt ASWs will be calculated using this channel open state. According to the calculation by García-Suárez *et al.*[39] the channel number of a Pt ASW composed of two to five atoms sandwiched between Pt electrodes is five.

F. Current-voltage curves of Pt NCs and ASWs

As shown in Fig. 11, the ratio of $G^{(2)}V^2$ and $G^{(3)}V^3$ to the total current is ~0.1%. In accordance with a first-principles calculation by Nielsen *et al.*,[13] a Pt single-atom contact with an interatomic distance of 0.29 nm shows a nonlinear current-voltage curve owing to modulation of the *d* orbitals by voltage-induced potentials.

The magnitude of $G^{(2)}$ increases when the upper part of the NC (the cantilever tip) tilts from the retraction direction, as shown in Fig. 7(b). However, no change was observed in $G^{(2)}$ when the wire tilted from the retraction direction, as shown in Fig. 7(f). In this case, the tip direction was maintained. $G^{(3)}$ is negative for the contact in Figs. 7(a)–7(h) and becomes larger as the conductance increases, showing that the deviation from a linear relationship increases as the contact size increases. Note that a small change in $G^{(3)}$ is observed when the wire tilts from the retraction direction, as shown in Fig. 7(f). For only the longest ASW in this observation [Fig. 7(h)], $G^{(3)}$ takes a positive value. Thus, this ASW has a different conductance feature against voltage increment. As discussed previously, we should consider the influence of hydrogen incorporation for this ASW.

V. CONCLUSION

We observed the structural dynamics of Pt ASWs during conductance feedback control by *in situ* HRTEM and simultaneously measured the force acting on them. Simple retraction of Pt NCs leading to transformation into ASWs was also performed, and the current-voltage curve was investigated for each atomic configuration. It was found that ASWs were stabilized at a tensile force of approximately 1 nN, showing that the observed ASWs were elongated elastically. The interatomic distance of the observed ASWs was 0.28 ± 0.03 nm. The elastic strain of the ASW with a length of four atoms was ~0.1, and the interatomic distance of the stress-free state was estimated as 0.25 nm.

Pt ASWs appeared when the feedback conductance was selected to be less than $3G_0$. The wire length increased to 0.54 ± 0.10, 0.80 ± 0.05, and 1.15 ± 0.05 nm as the feedback value was decreased to $2.2G_0$, $1.0G_0$, and $0.5G_0$. The contact transformed into NCs having a minimum cross-sectional width of two atoms. In the conductance histogram counted for the simple retraction process, one peak was observed at $1.3G_0$. Therefore, the conductance of ASWs was found to be less than $3G_0$, with $1.3G_0$ being that of the most-stable state. As shown in this study, *in situ* HRTEM directly links the atomic configuration to the mechanical and electrical properties of ASWs.

ACKNOWLEDGMENTS

This study was partly supported by funds from the Tanaka Kikinzoku Research Foundation, the Advanced Processing Mechanical Techniques Foundation, the Ogasawara Foundation for the Promotion of Science and Engineering, and Shimadzu Science Foundation, Grant-in-Aid for Scientific Research from the Japan Society for the Promotion of Science (Grants No. 18310075 and No. 19651047).

*kizuka@ims.tsukuba.ac.jp

[1] C. J. Muller, J. M. van Ruitenbeek, and L. J. de Jongh, Phys. Rev. Lett. **69**, 140 (1992).
[2] J. I. Pascual, J. Méndez, J. Gómez-Herrero, A. M. Baró, N. García, and V. T. Binh, Phys. Rev. Lett. **71**, 1852 (1993).
[3] N. Agraït, J. G. Rodrigo, and S. Vieira, Phys. Rev. B **47**, 12345 (1993).
[4] J. M. Krans, C. J. Muller, I. K. Yanson, T. C. M. Govaert, R. Hesper, and J. M. van Ruitenbeek, Phys. Rev. B **48**, 14721 (1993).
[5] G. Rubio, N. Agraït, and S. Vieira, Phys. Rev. Lett. **76**, 2302 (1996).
[6] C. Sirvent, J. G. Rodrigo, S. Vieira, L. Jurczyszyn, N. Mingo, and F. Flores, Phys. Rev. B **53**, 16086 (1996).
[7] J. L. Costa-Krämer, Phys. Rev. B **55**, R4875 (1997).
[8] J. L. Costa-Krämer, N. García, P. García-Mochales, P. A. Serena, M. I. Marqués, and A. Correia, Phys. Rev. B **55**, 5416 (1997).
[9] A. I. Yanson, G. R. Bollinger, H. E. van den Brom, N. Agraït, and J. M. van Ruitenbeek, Nature (London) **395**, 783 (1998).
[10] E. Scheer, N. Agraït, J. C. Cuevas, A. L. Yeyati, B. Ludoph, A. Martín-Rodero, G. R. Bollinger, J. M. Ruitenbeek, and C. Urbina, Nature (London) **394**, 154 (1998).
[11] B. Ludoph, M. H. Devoret, D. Esteve, C. Urbina, and J. M. van Ruitenbeek, Phys. Rev. Lett. **82**, 1530 (1999).
[12] G. Rubio-Bollinger, S. R. Bahn, N. Agraït, K. W. Jacobsen, and S. Vieira, Phys. Rev. Lett. **87**, 026101 (2001).
[13] S. K. Nielsen, M. Brandbyge, K. Hansen, K. Stokbro, J. M. van Ruitenbeek, and F. Besenbacher, Phys. Rev. Lett. **89**, 066804 (2002).
[14] C. Untiedt, A. I. Yanson, R. Grande, G. Rubio-Bollinger, N. Agraït, S. Vieira, and J. M. van Ruitenbeek, Phys. Rev. B **66**, 085418 (2002).
[15] N. García, M. Bai, Y. Lu, M. Muñoz, H. Cheng, and A. P. Levanyuk, J. Phys: Condens. Matter **19**, 016212 (2007).
[16] U. Landman, W. D. Luedtke, N. A. Burnham, and R. Colton, Science **248**, 454 (1990).
[17] M. Brandbyge, J. Schiøtz, M. R. Sørensen, P. Stoltze, K. W. Jacobsen, J. K. Nørskov, L. Olesen, E. Laegsgaard, I. Stensgaard, and F. Besenbacher, Phys. Rev. B **52**, 8499 (1995).
[18] L. Olesen, E. Lægsgaard, I. Stensgaard, F. Besenbacher, J. Schiøtz, P. Stoltze, K. W. Jacobsen, and J. K. Nørskov, Phys. Rev. Lett. **72**, 2251 (1994).
[19] A. M. Bratkovsky, A. P. Sutton, and T. N. Todorov, Phys. Rev. B **52**, 5036 (1995).
[20] J. L. Costa-Krämer, N. García, P. García-Mochales, and P. A. Serena, Surf. Sci. **342**, L1144 (1995).
[21] J. M. Krans, J. M. van Ruitenbeek, V. V. Fisun, I. K. Yanson, and L. J. de Jongh, Nature (London) **375**, 767 (1995).
[22] N. Agraït, G. Rubio, and S. Vieira, Phys. Rev. Lett. **74**, 3995 (1995).
[23] J. I. Pascual, J. Méndez, J. Gómez-Herrero, A. M. Baró, N. Garcia, U. Landman, W. D. Luedtke, E. N. Bogachek, and H.-P. Cheng, Science **267**, 1793 (1995).
[24] C. Zhou, C. J. Muller, M. R. Deshpande, J. W. Sleight, and M. A. Reed, Appl. Phys. Lett. **67**, 1160 (1995).
[25] U. Landman, W. D. Luedtke, B. E. Salisbury, and R. L. Whetten, Phys. Rev. Lett. **77**, 1362 (1996).
[26] A. G. Scherbakov, E. N. Bogachek, and U. Landman, Phys. Rev. B **53**, 4054 (1996).
[27] T. N. Todorov and A. P. Sutton, Phys. Rev. Lett. **70**, 2138 (1993).
[28] J. A. Torres, J. I. Pascual, and J. J. Sáenz, Phys. Rev. B **49**, 16581 (1994).
[29] K. Yuki, S. Kurokawa, and A. Sakai, Jpn. J. Appl. Phys., Part 1 **39**, 4593 (2000).
[30] R. H. M. Smit, C. Untiedt, A. I. Yanson, and J. M. van Ruitenbeek, Phys. Rev. Lett. **87**, 266102 (2001).
[31] K. Yuki, S. Kurokawa, and A. Sakai, Jpn. J. Appl. Phys., Part 1 **40**, 803 (2001).
[32] R. H. M. Smit, Y. Noat, C. Untiedt, N. D. Lang, M. C. van Hemert, and J. M. van Ruitenbeek, Nature (London) **419**, 906 (2002).
[33] S. K. Nielsen, Y. Noat, M. Brandbyge, R. H. M. Smit, K. Hansen, L. Y. Chen, A. I. Yanson, F. Besenbacher, and J. M. van Ruitenbeek, Phys. Rev. B **67**, 245411 (2003).
[34] V. Rodrigues, J. Bettini, P. C. Silva, and D. Ugarte, Phys. Rev. Lett. **91**, 096801 (2003).
[35] S. Csonka, A. Halbritter, G. Mihály, O. I. Shklyarevskii, S. Speller, and H. van Kempen, Phys. Rev. Lett. **93**, 016802 (2004).
[36] C. Untiedt, M. J. Caturla, M. R. Calvo, J. J. Palacios, R. C. Segers, and J. M. van Ruitenbeek, Phys. Rev. Lett. **98**, 206801 (2007).
[37] T. Shiota, A. I. Mares, A. M. C. Valkering, T. H. Oosterkamp, and J. M. van Ruitenbeek, Phys. Rev. B **77**, 125411 (2008).
[38] L. de la Vega, A. Martin-Rodero, A. Levy Yeyati, and A. Saúl, Phys. Rev. B **70**, 113107 (2004).
[39] V. M. García-Suárez, A. R. Rocha, S. W. Bailey, C. J. Lambert, S. Sanvito, and J. Ferrer, Phys. Rev. Lett. **95**, 256804 (2005).
[40] T. Kizuka and N. Tanaka, Philos. Mag. Lett. **69**, 135 (1994).
[41] T. Kizuka, K. Yamada, S. Deguchi, M. Naruse, and N. Tanaka, Phys. Rev. B **55**, R7398 (1997).
[42] T. Kizuka, Phys. Rev. Lett. **81**, 4448 (1998).
[43] H. Ohnishi, Y. Kondo, and K. Takayanagi, Nature (London) **395**, 780 (1998).
[44] V. Rodrigues, T. Fuhrer, and D. Ugarte, Phys. Rev. Lett. **85**, 4124 (2000).
[45] D. Erts, H. Olin, L. Ryen, E. Olsson, and A. Thölén, Phys. Rev. B **61**, 12725 (2000).
[46] T. Kizuka, H. Ohmi, T. Sumi, K. Kumazawa, S. Deguchi, M. Naruse, S. Fujisawa, S. Sasaki, A. Yabe, and Y. Enomoto, Jpn. J. Appl. Phys., Part 2 **40**, L170 (2001).
[47] V. Rodrigues and D. Ugarte, Phys. Rev. B **63**, 073405 (2001).
[48] S. B. Legoas, D. S. Galvão, V. Rodrigues, and D. Ugarte, Phys. Rev. Lett. **88**, 076105 (2002).
[49] T. Kizuka, Y. Takatani, K. Asaka, and R. Yoshizaki, Phys. Rev. B **72**, 035333 (2005).
[50] T. Kizuka, Phys. Rev. B **77**, 155401 (2008).
[51] R. H. M. Smit, C. Untiedt, G. Rubio-Bollinger, R. C. Segers, and J. M. van Ruitenbeek, Phys. Rev. Lett. **91**, 076805 (2003).
[52] K. Koizumi, Y. Oshima, Y. Kondo, and K. Takayanagi, Ultramicroscopy **88**, 17 (2001).
[53] S. R. Bahn and K. W. Jacobsen, Phys. Rev. Lett. **87**, 266101 (2001).
[54] D. Djukic, K. S. Thygesen, C. Untiedt, R. H. M. Smit, K. W. Jacobsen, and J. M. van Ruitenbeek, Phys. Rev. B **71**, 161402(R) (2005).
[55] M. Kiguchi, R. Stadler, I. S. Kristensen, D. Djukic, and J. M. van Ruitenbeek, Phys. Rev. Lett. **98**, 146802 (2007).